20

Compact CPW Metamaterial Resonators for High Performance Filters

Ibraheem A. I. Al-Naib[1], Christian Jansen[1] and Martin Koch[2]
[1]*Technische Universität Braunschweig*
[2]*Philipps-Universität Marburg*
Germany

1. Introduction

Since the origin of physics, scientists were concerned with the interaction of electromagnetic waves with matter. The electromagnetic properties of a material are commonly described by the electric permittivity epsilon (ε) and the magnetic permeability (μ). Soon it occurred that these dielectric parameters would have to be complex quantities to account for propagation losses and phenomena such as birefringence showed that they would have to be considered tensors in order to describe anisotropic behaviour.
Recently, the invention of artificial materials, which consist of periodically arranged, resonant, metallic sub-wavelength elements, led to a new class of materials offering a custom tailored dielectric response in certain frequency bands of interest. Today, many applications benefit from the unique electromagnetic properties that such artificial materials, also called metamaterials (MTM), offer. Especially planar metamaterials, which are easily facilitated into existing microwave circuitry, are of high practical interest, e.g. for high performance filters, antennas, and other microwave devices (Caloz & Itoh, 2005, Eleftheriades & Balmain, 2005, Marques et al., 2008). Aside from the device performance, miniaturization is a key issue in the design of metamaterial resonators, as a high integration density is a mandatory prerequisite to compete in mass-markets such as wireless communications.
In this book chapter, we will review some recently proposed planar metamaterial resonator concepts, illuminating their strengths and weaknesses in comparison to existing approaches, e.g. the ones discussed in (Marques et al., 2008). We will focus on structures integrated on coplanar waveguides (CPW) as this technology offers some distinct design advantages compared to conventional microstrip lines, e.g. the easy realization of shunts and the possibility of mounting active and passive lumped components (Simons, 2001, Wolff, 2006).
The remainder of this chapter is structured as follows. We will start with a short introduction to metamaterials and discuss some of the most prominent applications. After this general section, we will focus on CPW based metamaterial filter concepts.
The first concept which falls under this category is the complementary split ring resonator (CSRR) with and without bandwidth modifying slots, as introduced in (Ibraheem & Koch, 2007). These resonators provide a distinct stopband characteristic, which can be adjusted by

modifying the slot lengths, offering great design flexibility. However, the stopband response suffers from a spurious rejection band close to the main resonance, which has its origin in the differing electrical lengths of the inner and the outer resonator arm. This issue leads us to the complementary u-shaped split resonator (CUSR) (Al-Naib & Koch, 2008a), which cancels the spurious resonance by equalizing the electrical length of both resonator arms. Furthermore we will show that by combining a CSRR and a split ring resonator with strip lines in series, compact bandpass filters can be obtained, which could be very useful, e.g. in front end filter designs (Al-Naib et al., 2008).
Apart from the CSRR based structures, we will also discuss circular multiple turn complementary spiral resonators (CSRs) (Al-Naib & Koch, 2008b), which enable extremely small electrical footprint filters as each turn elongates the effective resonator length, thus lowering the resonance frequency.

1.1 The basics of Metamaterials

To better understand what sets metamaterials apart from ordinary media, Fig. 1 illustrates a schematic with μ and epsilon on the x- and the y-axis, respectively.

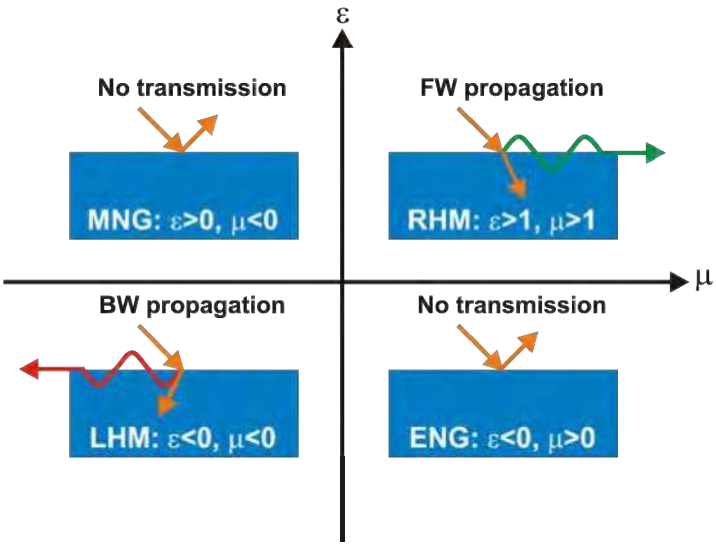

Fig. 1. Material classification.

Four regimes can be identified: The best known is the one where both ε and μ assume values larger than one. Most materials encountered in nature fall inside this upper right quadrant and are also referred to as right-handed media (RHM) or double positive material (DPS). Exceptions are ferrites, which are found in the upper left quadrant. In these materials μ becomes negative (MNG) while epsilon remains at positive values. The inverse scenario, where epsilon is negative (ENG) while μ remains positive is found in plasmas, which are grouped in the lower right corner of Fig. 1. The untapped lower-left corner contains left-handed materials, not yet discovered in nature.

Metamaterials can access all above mentioned regimes, at least in a limited spectral region, enabling new exciting applications such as superlenses or cloaking devices but also improving existing ones such as filter or antenna structures. The basic idea behind metamaterials lies in the combination of electric and/or magnetic resonances in such a way that ε and μ take the desired values in a certain frequency band. To illustrate this approach, we will now discuss a negative ε and a negative μ metamaterial and then combine both to obtain a left-handed medium.

1.1.1 ENG Metamaterials

Practically, ENG metamaterials consists of thin metallic wires. In the late nineties of the last century, concepts similar to the one shown in Fig. 2a have been explored (Pendry et al., 1996). Pendry et al. showed that its behaviour can be explained by the plasma resonance inside the metallic rods (Pendry et al., 1996, Pendry et al., 1998). As illustrated in Fig. 2b, epsilon starts with negative values in the lower frequency range (and hence, only evanescent modes are allowed to propagate) and then transits to positive values in the higher frequency region, through the plasma frequency (f_{pe}). ENG structures with plasmonic response have been suggested for the realization of sub-wavelength antennas with enhanced radiation properties and waveguide miniaturization (Engheta & Ziolkowski, 2006, Erentok & Ziolkowski, 2005, Gay-Balmaz et al., 2002, Hrabar et al., 2005).

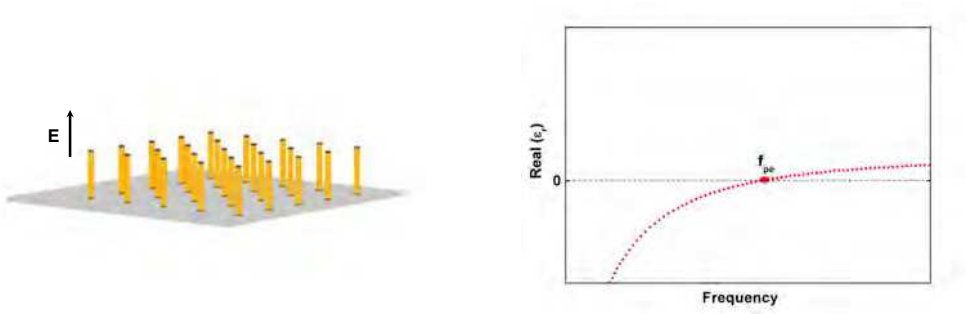

(a) (b)

Fig. 2. Wire medium with an applied electric field along the axes of the wires (a) and its effective electric permittivity value (b).

1.1.2 MNG Metamaterials

Aside from his work on metallic wire media, Pendry also proposed a novel type of magnetically excited resonator, the so called Split Ring Resonator (SRR), as shown in Fig. 3a (Pendry et al., 1999). The resonator consists of a pair of concentric rings, with slits etched in two opposing sides. By adequately exciting the SRR with a time varying magnetic field in the axial direction, a strongly resonant magnetic response can be observed as depicted in Fig. 3b.

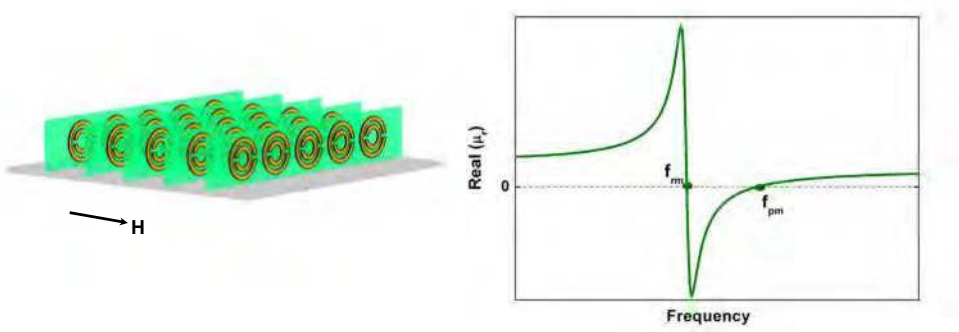

(a) (b)

Fig. 3. SRRs medium with magnetic field along their axis (a) and its analytical calculation of the effective magnetic permeability value (b).

1.1.3 LHM Metamaterial

In 2000, Smith et al. combined both the metallic wire ENG and the split ring resonator MNG media and were the first to experimentally observe a LHM (Shelby et al., 2001, Smith et al., 2000). Fig. 4a depicts a schematic of the prominent structure employed for these initial experiments. Fig. 4b shows the effective real part of ε and μ for the wire array and SRRs, respectively. f_{pe} and f_{pm} are the electric and magnetic plasma frequency while f_{rm} is the magnetic resonance frequency of the SRRs. The shaded area marks the resulting bandwidth between f_{rm} and f_{pe} for which a left handed behaviour with a negative effective refractive index is obtained.

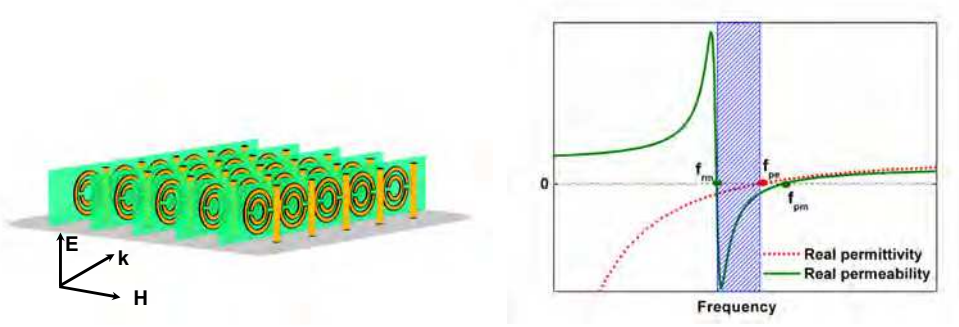

(a) (b)

Fig. 4. (a) Schematic of the LHM, resulting from the combination of an array of SRR particles with an array of thin wires (b) real part of effective permittivity (dotted) and permeability (solid) versus frequency.

1.2 Applications for metamaterials

In this section, we will briefly review the most prominent of the manifold suggested applications for metamaterials, in each case giving a short explanation of the benefit metamaterials can offer.

1. **Superlens -** Pendry proposed that a slab of LHM can be used as a lens which is free from all aberrations observed in a lens made with positive refractive index (Pendry, 2000). However, it was shown that very small deviations of the material parameters from the ideal conditions could lead to the excitation of resonances that cause deterioration of the performance of the lens. Nevertheless, scientists have been working to overcome different difficulties to improve the resolution (Ramakrishna & Grzegorczyk, 2008).
2. **Cloaking -** Another natural application for metamaterials is the development of gradient index media (Smith et al., 2005) because the value of the permittivity and permeability can be engineered at any point within the structure by adjusting the scattering properties of each unit cell (Driscoll et al., 2006, Greegor et al., 2005). By implementing complex gradients independently in the permittivity and permeability tensor components, it has been shown that an entirely new class of materials can be realized by the process of transformation optics (Leonhardt, 2006, Pendry & Smith, 2006). A recent example utilized metamaterials to form an "invisibility cloak" that was demonstrated to render an object invisible to a narrow band of microwave frequencies (Schurig et al., 2006).
3. **Scattering reduction** - metamaterials can be used for the reduction of electromagnetic wave scattering (Lagarkov & Kisel, 2001, Pacheco et al., 2002, Alu & Engheta, 2005). Recently a theoretical analysis based on Mie scattering was presented in (Alu et al., 2005) which indicated that metal, coated with metamaterials, has a drastically reduced scattering coefficient.
4. **Novel microwave components -** metamaterials can be employed as sub-wavelength resonators and zero phase delay lines. The advantage over that of RHM materials is the very small dimension of the resonator (Eleftheriades et al., 2004, Engheta, 2002). Moreover, low ε metamaterials can be employed to build high-gain antennas (Feresidis et al., 2005, Wang et al., 2006). Furthermore, compact antennas are realizable utilizing artificial magnetic conductors.

In the remainder of this chapter we will focus on planar metamaterials for planar microwave devices. The two main concepts for such metamaterials will be discussed in the following section.

2. Planar Microwave Metamaterials – A Brief Review

In order to bring metamaterial technology to microwave components, compatibility with planar circuit technology is mandatory. Two approaches have been introduced to meet this challenge: The first one employs a transmission line with integrated capacitive and inductive elements while the second one relies on planar metamaterial resonators loaded to a coplanar waveguide.

2.1 Transmission Line approach

A transmission line, loaded with reactive elements, such as capacitors and inductors, can be designed to exhibit capacitive effective series impedance while the effective shunt impedance remains inductive. The main advantage of such concept is its compatibility with conventional planar circuits. Fig. 5a illustrates the transmission line model of a TL-based metamaterials and Fig. 5b shows one of the proposed implementations (Caloz & Itoh, 2002). Several applications of TL-based metamaterials have been proposed and experimentally validated. For more information, the inclined reader is referred to (Caloz et al., 2002, Iyer & Eleftheriades, 2002, Oliner, 2002).

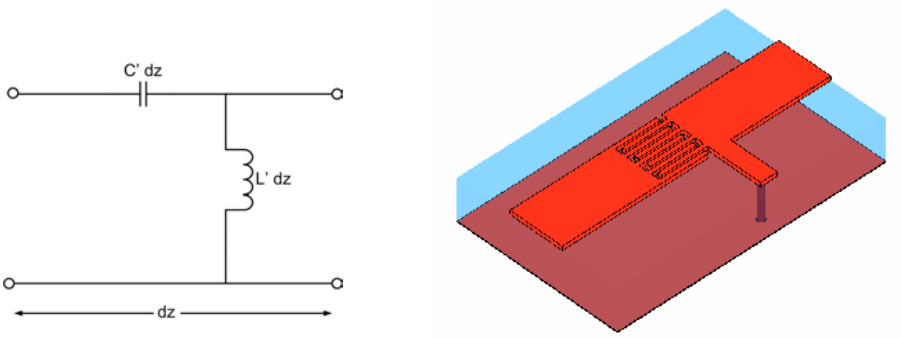

Fig. 5. Transmission line model for a TL-based metamaterials (a) and the proposed implementation (b).

2.2 CPW Approach

Coplanar waveguide technology offers a variety of advantages over the conventionally employed microstrip line. Among the benefits is the easy facilitation of shunts as well as the series surface mounting of active and passive devices. Furthermore, due to the absence of a ground plane a single metallization layer suffices which leads to reduced fabrication costs compared to microstrip technology.

Magnetic resonator structures, such as the SRR, can be employed as metamaterials if the exciting H-field is normal to the plane containing the resonator. In this operation mode, the induced currents will lead to the desired resonance of the magnetic permeability. Fig. 6 depicts the electric (E-) field and magnetic (H-) field in a CPW line. In the vicinity of the gaps lies an area where the H-field is normal to the CPW plane. Integrating magnetic resonators in this location should yield an efficient excitation, enabling a planar metamaterial structure. In the following we will discuss different implementations of this basic concept.

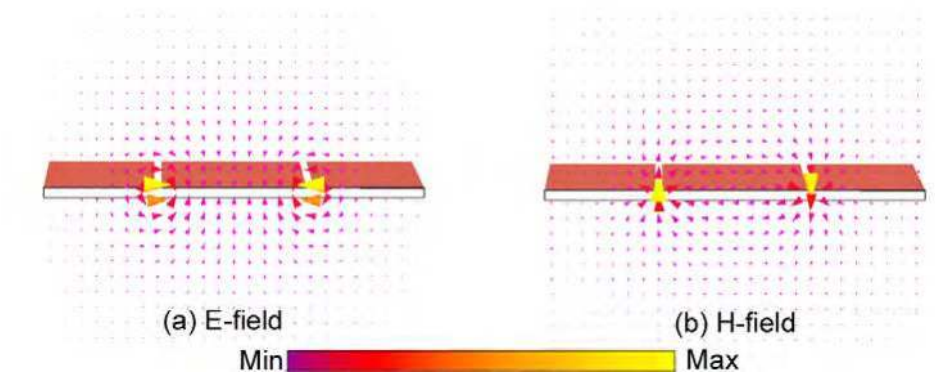

Fig. 6. The transverse electric- (a) and magnetic- (b) field in CPW.

A first implementation of a single metallization layer, CPW-based planar design introduced the SRRs directly on the slots of the CPW as depicted in the inset of Fig. 7a (Falcone et al., 2004). The gaps of the CPW are broadened to provide enough space to hold the SRRs. The SRRs are excited magnetically because the magnetic field is confined to the gaps. Fig. 7b shows the numerically obtained transmission parameters. The transmission depicts bandstop behaviour due to the magnetic resonance. Unfortunately, with regards to the return loss, the performance is quite poor because the structure is highly mismatched since the CPW line impedance is the ratio between the central conductor width and the air gap separation. Therefore, having the SRRs inside the slots of CPW puts tight restrictions to the line impedance.

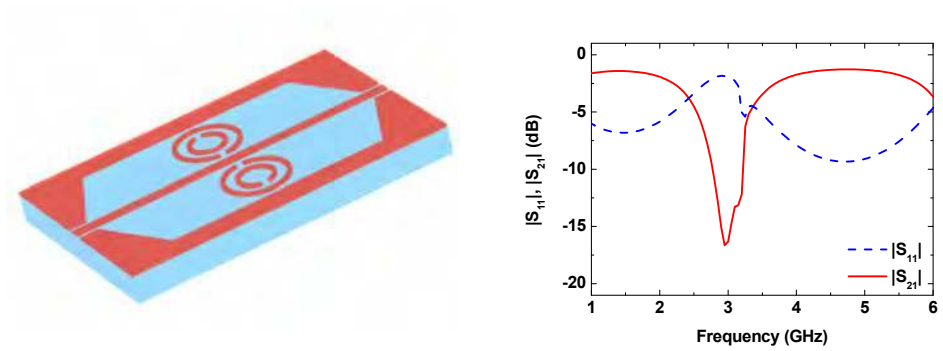

(a) (b)

Fig. 7. Single metallized CPW with SRRs inside the slots (a) and its S-parameters (b).

To overcome the mismatch problem, another approach has been proposed. Here, the SRRs are placed on the bottom side of the dielectric layer as shown in Fig. 8a (Martin et al., 2003a). In this case, the CPW can be designed to have almost the same impedance as if no SRRs were present. Four unit cells are needed to achieve good behaviour as shown in Fig. 8b.

However, the advantage of having a single metal layer is no longer maintained, reducing the applicability of this concept.

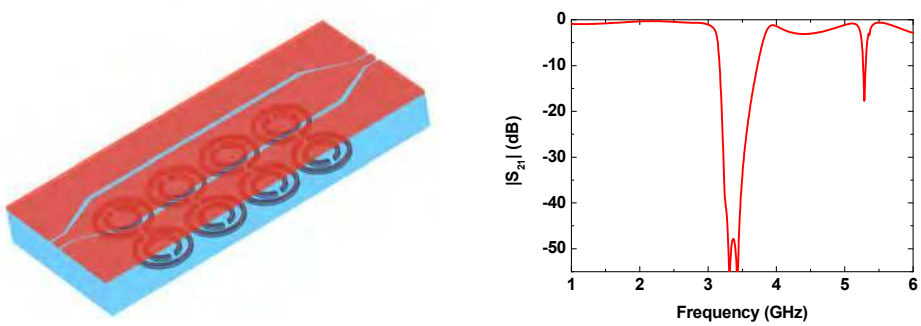

(a) (b)

Fig. 8. CPW with backside loaded SRRs (a) with its transmission characteristic (b).

3. Planar Microwave Metamaterials – Recent Advances

This section reviews novel planar metamaterial resonator concepts which have recently been proposed. The first concept is the complementary split ring resonator (CSRR). Unlike the structures introduced in sec. 3.1, which consist of two metal layers, the CSRRs have been integrated into the CPW layer to maintain the advantages single layered structures offer. However, the stopband response suffers from a spurious rejection band close to the main resonance. To resolve this issue, the complementary u-shaped split resonator (CUSR) discussed in section 3.2, which cancels the spurious resonance, has been introduced. Apart from the CSRR based structures, circular multiple turn complementary spiral resonators (CSRs) are discussed in section 3.4, which feature an extremely small electrical footprint as each turn elongates the effective resonator length. Finally, combining a CSRR and an SRR with strip lines in series leads to compact bandpass filters introduced in section 3.5. Such devices could be very useful, e.g. in front-end filter designs.

3.1 The Novel CSRR/CPW

As neither of the designs discussed in section 2.2 could satisfy the demand for an impedance matched, single layered, planar metamaterial, a new concept had to be developed. At the core of this concept stands the integration of complementary SRRs (CSRRs) into a CPW making use of the Babinet principle which leads to the structures shown in Fig. 9a & 9b. For clarity's sake, we will limit the discussion in this work to a single CSRR pair. However, cascading of the CSRRs is possible, resulting in even better performance. At the edges of the structure we added the CPW tapers to exclude measurement errors due to soldering connectors to the devices. The taper function was verified through simulation and experiment to provide maximum matching between the two sides of the CPW. A standard mask/photoetching technique is used to fabricate the structures using an FR-4 substrate (dielectric constant $\varepsilon_r = 4$, loss tangent $\tan\delta = 0.02$, thickness $h = 0.5$ mm). With a single pair

of CSRRs we obtain a considerably higher suppression than reported in (Martin et al., 2003a).

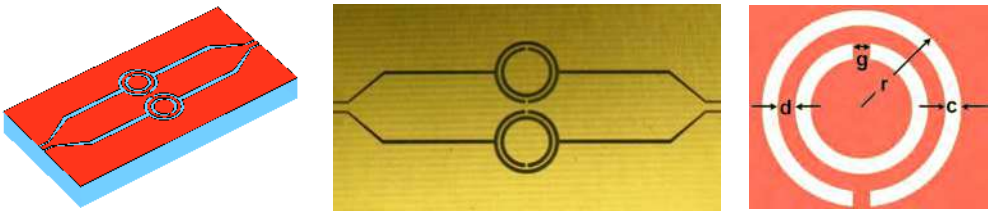

(a) (b) (c)

Fig. 9. (a) 3D layout of CPW/CSRR structure (b) top-view of the fabricated structure (c) schematic of CSRR with its dimensions.

First, a simulation of a single unit cell with periodic boundary conditions in propagation direction is performed using the Eigenmode solver of CST Microwave studio (CST). The dimensions of the unit cell are illustrated in the inset of Fig. 9c. An external radius of r = 3.6 mm, a width of c = 0.27 mm, a separation of d = 0.43 mm, and a length of the "metallic bridge" g = 0.43 mm are chosen so that the structures operate in the C-band. Calculating the dispersion by varying the phase shift in propagation direction between 0° and 180° reveals a photonic band gap between 4.2 GHz and 5.6 GHz (c.f. Fig. 10a). This bandgap is produced by the complementary rings which exhibit an effective negative dielectric permittivity. Hence, a stopband behaviour in the transmission magnitude with a centre frequency around 4.9 GHz is expected.

We use Ansoft HFSS software (HFSS) (a 3D full-wave solver based on the finite element method with adaptive iterative meshing) to simulate the transmission through the structures with a very high mesh resolution by specifying the maximum change in the S-parameters between two successive iterations to be 0.3%. Furthermore, a fine discrete sweep with a 0.02 GHz step size for the band between 4.5-5.5 GHz is performed, where sharp spectral transients are expected. The simulated magnitude response (dotted line) for the insertion loss is shown Fig. 10b. The insertion loss for the CSRR structure shows the expected stopband behaviour close to 5 GHz. Between 4.6 GHz and 5.5 GHz, an attenuation higher than 10 dB is achieved, which is in good agreement with the dispersion analysis.

An HP E8361A vector network analyzer (VNA) with a microstrip test fixture (Wiltron 3680) is employed to identify the S-parameters of the fabricated structure in the frequency band between 2 and 10 GHz. A thru-short-line (TRL) kit was used to calibrate the system. For the whole band of interest, the return loss is better than 28 dB. The measurements of the fabricated structure are shown in Fig. 10b (solid line). A good agreement between the measured S-parameters and the simulated HFSS results, confirming the dispersion analysis carried out with CST MWS. The small shifts in the resonance frequency can be ascribed to inhomogeneities in the ring dimensions.

Beneath the low-frequency limit of the artificial band gap, the structure exhibits excellent matching without any significant insertion loss. In the upper passband a good performance up to 7 GHz is achieved, but for higher frequencies (shaded area in Fig. 10) a spurious

resonance leads to an undesired dip in the transmission response at 9.1 THz. The origin of this dip and countermeasures to remove it are discussed in the following section.
Another remarkable aspect about the CSRR is the high rejection level in the forbidden band of nearly 30 dB, which is at least twice as high as the suppression of the SRR-based structures introduced in (Martin et al., 2003a). Thus, CSRRs provide an effective way to eliminate frequency parasitics in CPW structures. By cascading multiple CSRR unit cells even higher suppression levels can be achieved.

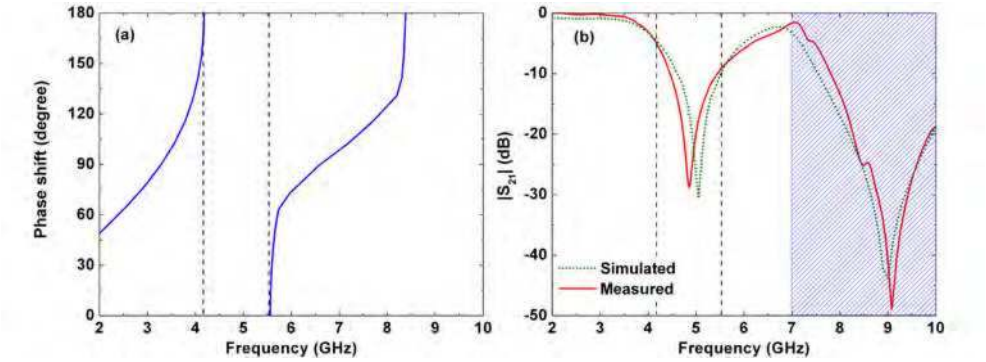

Fig. 10. (a) Dispersion analysis (b) simulated and measured insertion loss.

3.2 U-shaped resonators – Overcoming the spurious resonance

In the last section, we discussed the CPW-integrated CSRRs for use as a single metallization layer, high rejection stop band filter. Yet, the insertion loss of the CPW-CSRR suffers from a strong spurious stopband located on the high frequency side very close to the actual stopband. This spurious resonance results from a phenomenon called differentiating resonances (Ibraheem et al., 2008). At the core of this problem lies the slight difference in the length of the inner and the outer resonator arms. Thus, we proposed complementary u-shaped split resonator (CUSR) which is depicted in Fig. 11a (Al-Naib & Koch, 2008a). Here, the physical length of the u-shaped outer and inner rectangular resonator is identical. Thus, the spurious resonance present in case of the CSRR filters should disappear, resulting in a flat and low-loss passband response.
To provide a benchmark for the CUSR resonator performance we compare its properties to the ones of a CSRR. Figs. 11b & 11c illustrate the layout of the CSRR and CUSR cells integrated on a tapered CPW transmission line. The top layer contains the resonators, which are fabricated in a wet etching process. The lattice constant is 9.6 mm, the centre conductor width 9.15 mm and the slot width 0.45 mm. After the taper, the dimensions of the centre conductor and the slot width are 1 mm and 0.14 mm, respectively. The resulting characteristic impedance for the host line is Z0 = 50 Ohm. The CPW taper, which eliminates errors due to soldered connectors, was optimized for maximum matching between the two sides of the CPW. All structures are fabricated on an FR-4 substrate (dielectric constant ε_r = 4, loss tangent tanδ = 0.02, thickness h = 0.5 mm, and double sided copper clad of 35μm) using an in-house standard mask/photoetching technique.
In a next step we determined the S-parameters of the resonators within the frequency band of 1 to 12 GHz using an HP E8361A vector network analyzer (VNA) with a microstrip test

fixture (Wiltron 3680). As already explained in the previous section, a thru-short-line (TRL) calibration was performed for the CPW. The return loss was found to be better than 31 dB for the whole band of interest. Fig. 11a depicts the dimensions of the CUSR employed in this study. We have chosen an external radius of r = 3.6 mm, a separation of c = 0.4 mm, a width of d = 0.4 mm, and a metallic strip g = 0.4 mm for operation in the C-band. Figs. 11b & 11c show the fabricated structures for both CPW/CSRR & CPW/CUSR. In case of the CUSR, the resonator arm length for both u-shaped arms is identical in this design.

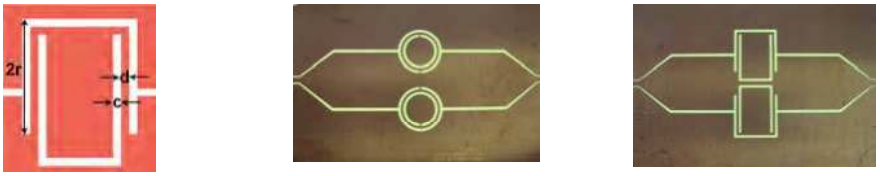

(a) (b) (c)

Fig. 11. (a) Schematic of CUSR with its dimensions and layout of CPW/CSRR structure (b) and CPW/CUSR (c).

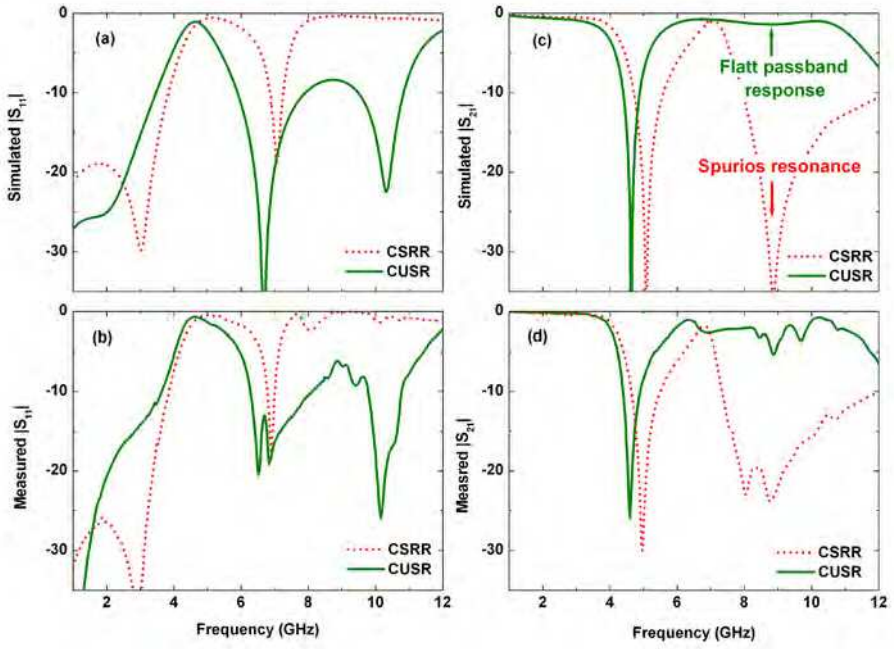

Fig. 12. Simulated (a) and measured (b) return loss for CPW-CSRR and CPW-CUSR structures. Simulated (c) and measured (d) insertion loss for CPW-CSRR and CPW-CUSR structures.

To simulate the transmission frequency response of the structures we use a commercially available 3D full-wave solver based on the finite element method (HFSS). Fig. 12 shows the simulated and measured magnitudes of the return and insertion losses of both CSRR (dashed line) and CUSR (solid line) structures. The primary stopband where the real part of

the electric permittivity is expected to be negative is clearly pronounced in both cases. The simulated and measured return loss is shown in Figs. 12a and 12b. In case of the CSRR, the upper passband still has a considerable attenuation due to the spurious resonance induced by the differing length of the inner and the outer resonator as aforementioned in the previous section. In this upper passband the return loss of the CUSR is approximately 8 dB lower than that of the CSRR, offering a drastically improved stopband filter performance.
Figs. 12c and 12d depict the simulated and measured insertion loss. The stopbands are centred at approximately 4.6 GHz and 5.1 GHz for CUSR and CSRR, respectively. Although, both structures feature very high rejection levels and sharp transition edges, the previously mentioned spurious extended stopband centred around 8.8 GHz limits the applicability of the CSRR resonators. The measured data for the return and insertion losses agree well with the simulated results. The small discrepancies can be attributed to geometrical inhomogeneities introduced by the wet etching process. Please note that in addition to the improved filter performance the resonance frequency of the CUSRs is 10% less compared to the CSRRs, enabling a higher degree of miniaturization. For a thorough parametric study of the geometrical dimensions with regards to the resonance behaviour of the structures, the inclined reader is referred to (Al-Naib & Koch, 2008a).

3.3 Bandwidth modifying slots

We will now take a short excurse to an interesting alteration of the resonator geometry: It has been shown, e.g. in (Ibraheem & Koch, 2007), that slots inserted in the vicinity of a resonator can modify its bandwidth, enabling a simple method of custom tailoring filters to specific applications. To investigate this aspect for the CSRR and CUSR structures we fabricated structures as depicted in Fig. 13 with slots of 0.8 mm width and differing lengths close to the metamaterial resonators. The slot length *sl* varies from 0 to 3.6 mm in increments of 0.6 mm. Fig. 13b shows the bandwidth over the *sl* parameter. A continuous increase of the bandwidth with the length of the slots is observed for both structures. It is worth mentioning that the structures are still in the sub-wavelength range despite the presence of the slots. To conclude, slots in the vicinity of CSRRs or CUSRs allow easy custom tailoring of the filter bandwidth without the need for a time consuming redesign of the resonator itself.

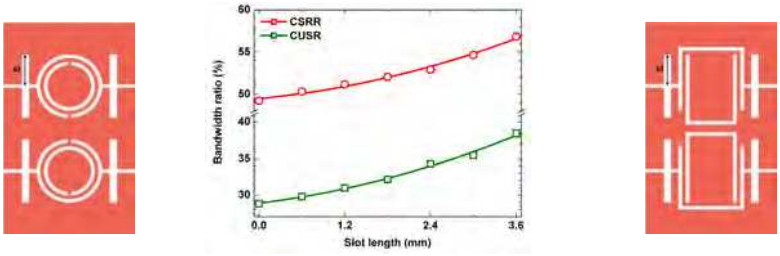

(a) (b) (c)

Fig. 13. (a) CPW-CSRR with nearby slots (b) bandwidth of the stop band filter vs. the slot length for CPW-CSRR and CPW-CSCR structures (c) CPW-CUSR with nearby slots.

3.4 Spiral CSRR/CPW

Many applications throughout microwave technology demand for a high degree of miniaturization. In order to meet this challenge, we will use this section to study the concept

of spiral resonators in conjunction with the previously discussed CPW integrated CSRRs and demonstrate the high miniaturization potential which arises from this combination. The spiral resonator was proposed to further reduce the size of the SRRs (Baena et al., 2004). We utilize the complementary split rectangle resonators (CSCR) and the Complementary Spiral Resonator (CSR) with multi turns to obtain single layer bandstop filters with a high degree of miniaturization.

The structures of interest are depicted in Fig. 14. It shows the layout of the tapered CPW incorporating a unit cell of CSRRs, CSCRs, and CSRs, respectively. The resonators are symmetrically etched into the top layer. The lattice constant a is 8 mm. The FR-4 substrate is employed for all the structures (dielectric constant ε_r = 4, loss tangent $\tan\delta$ = 0.02, and thickness h = 0.5 mm). They have an external radius of r = 3.6 mm, a separation of c = 0.2 mm, a width of d = 0.2 mm, and a metallic strip g = 0.2 mm (c.f. Fig. 9c).

To simulate the transmission frequency response, we use the commercial software package Ansoft HFSS (HFSS). Fig. 15 shows the simulated magnitude response for a CSRR, a CSCR and the new spiral CSRR. For all structures, there is a strong main stopband centred at 4.08 GHz, 3.36 GHz, and 1.38 GHz for the CSRR, CSCR, and the spiral CSRR, respectively. Please note that the resonance frequency of the spiral CSRR is only one-third compared to the resonance frequency of the CSRRs, revealing the high potential for miniaturization. Measurements, which are in good agreement with the simulations, are shown in Fig. 15b & 15d.

(a) (b) (c)

Fig. 14. Layout of the CPW/CSRR (a), CPW/CSCR (b) and CPW/CSR structures (c).

In order to achieve even higher degrees of miniaturization more turns can be added to the spiral resonators as shown in the insets of Fig. 16. We investigate two, four, six, and eight turn spiral resonators. However, increasing the number of turns not only reduces the resonance frequency (increasing the miniaturization) but also lowers the separation of the main stopband from the next higher frequency resonance. Fig. 16a depicts the dependence of the resonance frequency (Fig. 16a, left scale), the corresponding electrical size in terms of guided wavelength (Fig. 16a, right scale) and the frequency ratio of the second to the first resonance (Fig. 16b) on the number of spiral turns. Saturation in the change of the resonance frequency with increasing number of turns is revealed. This effect can be explained by the saturation of the resonator inductance and capacitance and has already been observed in (Bilotti et al., 2007). However, a very small electrical size of $\lambda g/50$ is achieved with an eight turn spiral resonator. The ratio between the fist and the second resonance, shown in Fig. 16b, decreases with the number of turns and also saturates at a value of approximately 2.2 for eight turns. Thus, in contrast to the CSRR structures discussed in the previous sections, the second resonance does not impact the excellent filter performance.

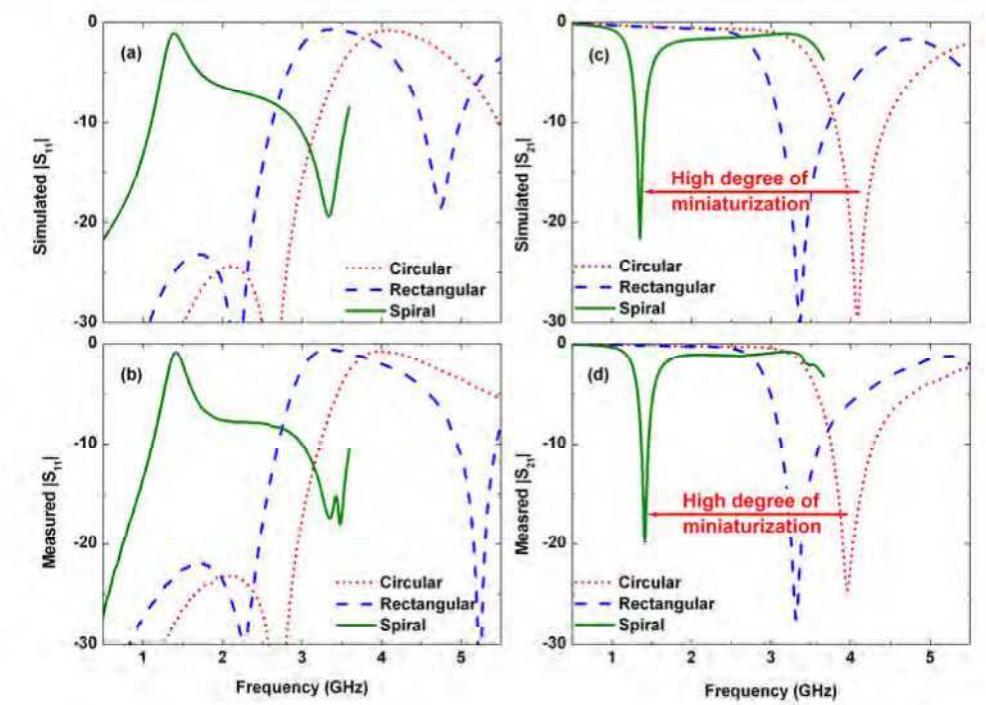

Fig. 15. Simulated (a) and measured (b) return loss for the CPW/CSRR (circular), CPW/CSCR (rectangular), and CPW/CSR (spiral) structures. Simulated (c) and measured (d) insertion loss for the CPW/CSRR (circular), CPW/CSCR (rectangular), and CPW/CSR (spiral) structures.

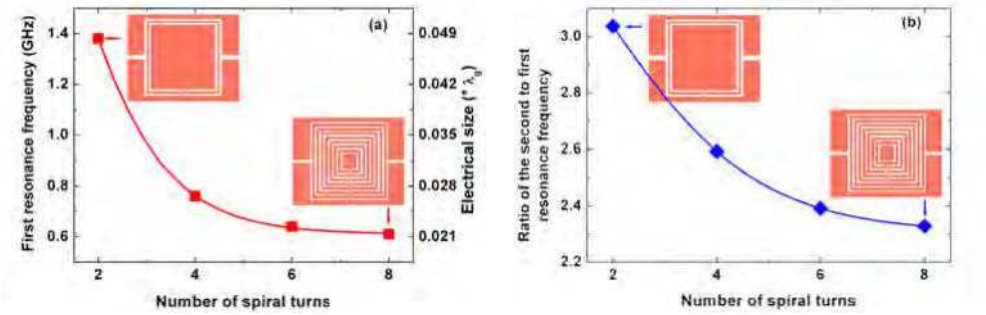

Fig. 16. (a) Resonance frequency versus number of spiral turns (b) ratio of the second to first resonance frequencies.

3.5 Bandpass Filter with CSRR/CPW

So far, we have presented how CSRRs can be employed to miniaturize conventional bandstop filters tremendously. Although bandstop filters are very important as mentioned earlier, many modern microwave applications, such as automotive radar and wireless

communication systems, rely on bandpass filters (BPFs). Moreover, transceiver modules are based on bandpass filters to separate uplink from downlink. In order to succeed in the field of wireless applications, miniaturization of these versatile devices is mandatory to achieve a high integration density in the overall system.

Martin et al. proposed a left-handed materials which consists of CPW loaded with SRRs from the backside of a substrate, in combination with periodically aligned strip lines (SLs) on the upside, connecting the central conductor to the ground planes (Martin et al., 2003b). The frequency response of such structure exhibits low insertion losses and a sharp cutoff at the lower band edge. However, the attenuation level above the passband is usually not as high as required for practical filter applications. A workaround for this problem is to increase the number of unit cells to achieve the desired attenuation at the upper transition band edge. Unfortunately, this increase directly leads to a higher insertion loss at the centre frequency as well, so that a trade-off has to be found.

This section presents a BPF based on combining conventional SRRs with CSRRs resonators. It exhibits low insertion loss, sharp cut-off and high stopband attenuation. CSRRs feature low pass characteristics compared to SRRs which exhibit high pass behavior. Combining both SRRs and CSRRs allows a very flexible design of BPFs. The lower and higher band edges are defined by the resonance frequency of the SRR and CSRR, respectively.

Fig. 17a depicts one of the fabricated structures where CSRR cascaded with SRR. The dimensions of the SRRs are chosen such that the device operates in the C-Band around 4 GHz. Figs. 17b & 17c shows the dimensions of both SRRs and CSRRs which have the same width of c = 0.42 mm, a separation of d = 0.38 mm and a gap of g = 0.36 mm. The outer radius r is 3.2 mm and 3.6 mm for the SRRs and CSRRs, respectively. A commercial low cost FR-4 substrate (dielectric constant ε_r = 4, loss tangent tanδ = 0.02, thickness h = 0.5 mm) is used to fabricate the structures.

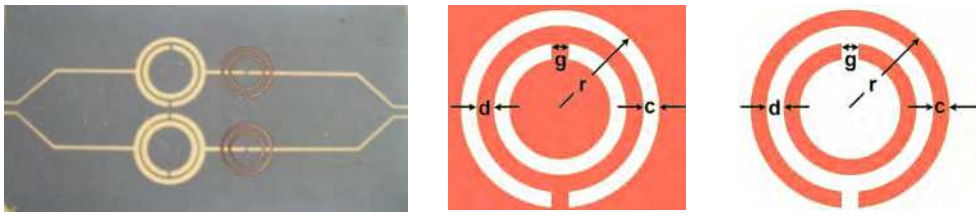

(a) (b) (c)

Fig. 17. (a) SRR/SL-CSRR loaded the CPW fabricated structure. Schematic of CSRR (b) and SRR (c) with relevant dimensions.

Three selected structures have been chosen for simulations and measurements. They include a unit cell of each, SRR/SL and CSRR as well as a combination of both. A commercially available 3D full-wave solver (HFSS) based on the finite element method is employed to calculate the S-parameters. Accompanying measurements were performed using a vector network analyzer (HP E8361A) with a microstrip test fixture (Wiltron 3680). The simulated phase for the three structures is given in Fig. 18. Examining the phase responses of the single elements and the overall structure shows the optimization options in terms of impedance matching. The phase response of the SRR/SL is mainly capacitive for the lower stopband. At the resonance frequency, a phase flip occurs, after which the SRR/SLs behave mainly inductive. The CSRR exhibits a gradually decreasing phase response over the whole

frequency band of interest. The behavior of the CSRR changes from inductive to capacitive at the centre frequency which helps to compensate for the high inductive reactance of the SRR/SL after their phase flip resulting in lower insertion loss in the passband.

Figs. 19 & 20 shows simulated and measured return (S_{11}) and insertion (S_{21}) losses, respectively. The simulations qualitatively agree very well with the measurements. Simulation and measurement graphs reveal only small quantitative discrepancies, which can be attributed to manufacturing inaccuracies. At the centre frequency, the measured and simulated return loss for the combined SRR/SL-CSRR is 18.9 and 17.6 dB, respectively. The simulated and measured insertion loss at the centre frequency of f_c = 4 GHz is 2.7 dB and 3.4 dB, respectively. The out-of-band rejection is higher than 19 dB in the simulation and 17 dB in the measurement. Keeping in mind, that the whole structure has a geometrical outline of only 0.29 λg by 0.29 λg (with λg as guided wavelength) and is based on standard FR-4 substrate material, the performance is superior to previously demonstrated devices which employ cascaded SRR cells.

Another investigation has been performed with a more expensive microwave substrate (Rogers RO3003, dielectric constant ε_r= 3, tanδ = 0.0013, thickness h= 0.127 mm). The simulation predicts a reduction of insertion loss by 60% (1.6 dB) and an out-of-band rejection enhancement of 4 dB. In order to obtain the same centre frequency of the FR-4 sample, the radius of the split rings was reduced to 2.8 mm to compensate for the difference in substrate thickness and the dielectric constant. Experimentally, we found a reduction in the insertion loss at the centre frequency of 55% (1.5 dB), which is close to the predicted value. The demonstrated design allows very narrow passbands usually only available for filters constructed in more expensive technologies, e.g. based on high-temperature superconductor thin films.

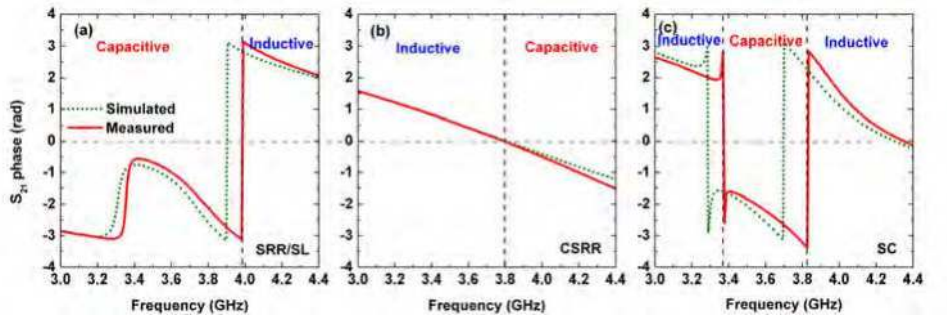

Fig. 18. Simulated and measured transmission phase for SRR/SL (a), CSRR (b) and both structures (c).

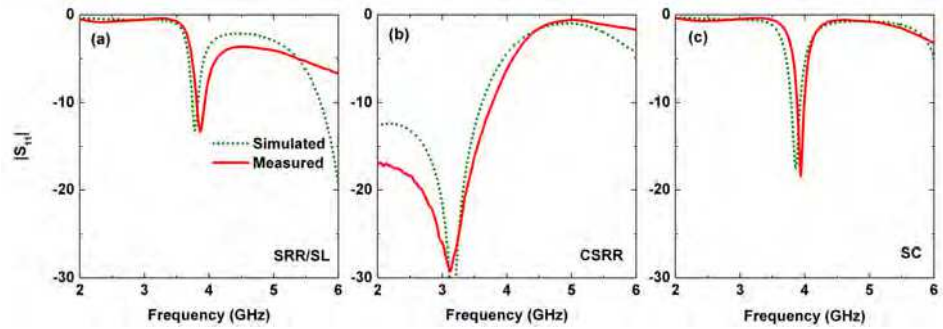

Fig. 19. Simulated and measured return loss for the SRR/SL (a), CSRR (b) and both structures (c).

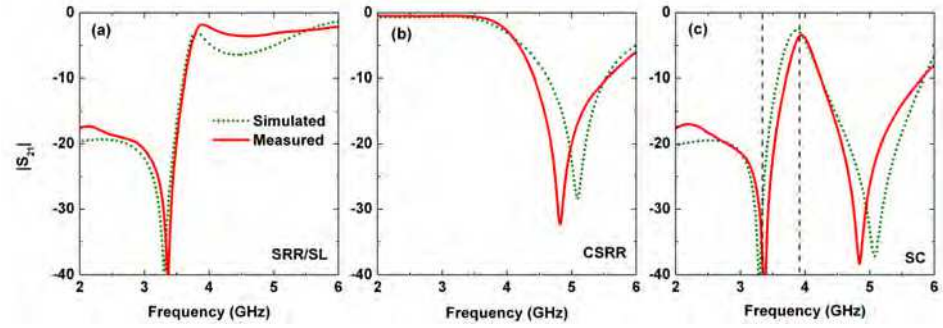

Fig. 20. Simulated and measured insertion loss for the SRR/SL (a), CSRR (b) and both structures (c).

Moreover, we analyzed the dependence of the insertion loss on the bandwidth ratio (for FR-4 and RO3003 substrates) in Fig. 21. The outer radius of the SRRs was swept from 3.0 mm to 3.6 mm and 2.6 mm to 3.2 mm in steps of 0.1 mm for the FR-4 and the RO3003, respectively. The resonance frequency of the SRRs is proportional to the inverse square root of the outer radius (Marques et al., 2002). Thus, the resonance frequency is decreased with an increase in the radius of the SRRs. This leads to a widening of the bandwidth of the overall structure. The bandwidth ratio is defined as the relation of the bandwidth over the centre frequency so that the bandwidth ratio is increased as well. As long as the centre frequency of the bandpass filter lies within the passband of both resonators, the influence of the insertion loss on the bandwidth ratio stays very small. While when the centre frequency of the bandpass filter lies in the transition region, reducing the bandwidth ratio a little further drastically increases the losses. For the current case, the losses remain low for bandwidth ratios of down to 10%. Hence, custom tailored filter designs can be achieved by varying only a single dimension of the structure, namely the outer radius of the SRRs. Additional SRR or CSRR cells could be added to improve the performance in case the required bandwidth ratio is below 10%. Moreover, multiple turn rectangular spiral resonators and its complementary could be employed to achieve a significant further miniaturization.

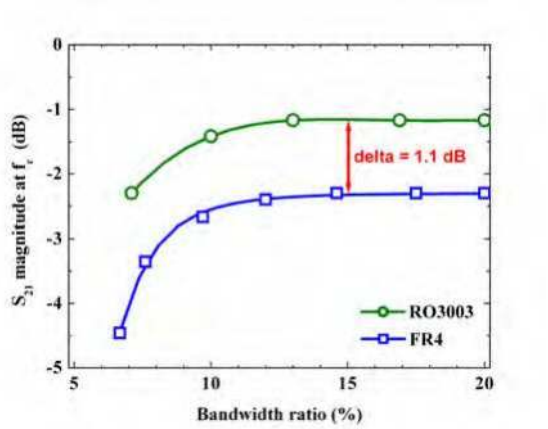

Fig. 21. Simulated S21 magnitude at the centre frequency versus the bandwidth ratio for a sweep of the outer radius of the SRR.

4. Conclusion

In conclusion we have discussed recent advances in the field of planar metamaterials. Especially, recently proposed planar metamaterial resonators for high performance, small footprint filters integrated in coplanar waveguide technology were considered. The following list, illuminating briefly the characteristic strengths and weaknesses of the previously discussed concepts, shall serve both as summary and reference to the inclined reader.

Complementary split ring resonator (CSRR) with slots
(Section 3.1, see also (Ibraheem & Koch, 2007))

+ Stopband filter
+ High stopband rejection
+ Low passband losses
+ Rather small outline dimensions
+ Slots allow custom-tailoring of the filter bandwidth
- Spurious resonance in the higher passband due to difference in inner and outer resonator arm length

U-shaped split resonator (CUSR)
(Section 3.2, see also (Al-Naib & Koch, 2008a))

+ Stopband filter
+ High stopband rejection
+ Low passband losses
+ Rather small outline dimensions
+ No spurious resonance in the higher passband due to equal resonator arm lengths

Combined CSRR/SRR with strip lines in series
(Section 3.5, see also (Al-Naib et al., 2008))

+ Bandpass filter
+ Low passband losses
+ High stopband rejection
+ Moderate outline dimensions
+ Well suited for frontend designs

Circular multiple turn complementary spiral resonators (CSRs)
(Section 3.4, see also (Al-Naib & Koch, 2008b))

+ Stopband filter
+ Extremely compact size
+ Low passband losses
+ High stopband rejection
+ Well suited for frequency selective surface designs with small resonator spacings
– Spurious resonance due to differing resonator arm lengths.
+ But: still a good separation between spurious resonance and main resonance is achieved

5. References

Al-Naib, I. A. I.; Jansen, C. & Koch, M. (2008). Miniaturized bandpass filter based on metamaterial resonators: a conceptual study, *Journal of Physics D: Applied Physics*, 41(20), 205002.

Al-Naib, I. & Koch, M. (2008a). Higher Degree of Miniaturization with Split Rectangle Resonators. *Proceedings of the 38th European Microwave Conference*, pp. 559-562, Amsterdam-The Netherlands.

Al-Naib, I. & Koch, M. (2008b). Miniaturization of Coplanar waveguide Bandstop Filter with Spiral Resonators, *Metamaterials'2008*, pp. 715-717, Pamplona-Spain.

Alu, A. & Engheta, N. (2005). Achieving transparency with plasmonic and metamaterial coatings, *Physical Review E*, 72(1), 016623.

Baena, J. D.; Marqués, R.; Medina, F. & Martel, J. (2004). Artificial magnetic metamaterial design by using spiral resonators, *Phys. Rev. B, Condens. Matter*, 69, pp. 014402(1)-014402(5).

Bilotti, F.; Toscano, A. & Vegni, L. (2007.) Design of spiral and multiple split-ring resonators for the realization of miniaturized metamaterial samples, *IEEE Trans. Microwave theory and technology*, 55, pp. 2258-2267.

Caloz, C. & Itoh, T. (2002). Application of the transmission line theory of left-handed (LH) materials to the realization of a microstrip "LH line". *IEEE Antennas and Propagation Society International Symposium*, 2, pp. 412-415.

Caloz, C. & Itoh, T. (2005). *Electromagnetic Metamaterials: Transmission Line Theory and Microwave Applications*, Wiley & Sons.

CST Microwave Studio®, http://www.cst.com.

Driscoll, T.; Basov, D. N.; Starr, A. F.; Rye, P. M.; Nemat-Nasser, S.; Schurig, D. & Smith, D. R. (2006). Free-space microwave focusing by a negative-index gradient lens. *Applied Physics Letters*, 88(8), 081101-3.

Eleftheriades, G. V. & Balmain, K. G. (2005). *Negative Refraction Metamaterials. Fundamental Principles and Applications*, Wiley & Sons.

Eleftheriades, G.; Grbic, A. & Antoniades, M. (2004). Negative-refractive-index transmission-line metamaterials and enabling electromagnetic applications. *IEEE Antennas and Propagation Society International Symposium*, 2, pp. 1399-1402.

Engheta, N. (2002). An idea for thin subwavelength cavity resonators using metamaterials with negative permittivity and permeability. *IEEE Antennas and Wireless Propagation Letters*, 1, pp. 10-13.

Engheta, N. & Ziolkowski, R. W. (2006). *Electromagnetic Metamaterials: Physics and Engineering Aspects*, Wiley & Sons.

Erentok, A. & Ziolkowski, R. (2005). Development of Epsilon-Negative (ENG) Metamaterials for Efficient Electrically Small Antenna Applications, *IEEE Antennas and Propagation Society International Symposium*, pp. 304-307, Washington, DC, USA.

Falcone, F.; Martin, F.; Bonache, J.; Marques, R. & Sorolla, M. (2004). Coplanar waveguide structures loaded with split-ring resonators, *Microwave and Optical Technology Letters*, 40(1), 3-6.

Feresidis, A.; Goussetis, G.; Shenhong, W. & Vardaxoglou, J. C. (2005). Artificial magnetic conductor surfaces and their application to low-profile high-gain planar antennas, *IEEE Transactions on Antennas and Propagation*, 53(1), 209-215.

Gay-Balmaz, P.; Maccio, C. & Martin, O. J. F. (2002). Microwire arrays with plasmonic response at microwave frequencies, *Applied Physics Letters*, 81(15), 2896-2898.

Greegor, R. B.; Parazzoli, C. G.; Nielsen, J. A.; Thompson, M. A.; Tanielian, M. H. & Smith, D. R. (2005). Simulation and testing of a graded negative index of refraction lens. *Applied Physics Letters*, 87(9), 091114-3.

HFSS™, available at http://www.ansoft.com/products/hf/hfss.

Hrabar, S.; Bartolic, J.; & Sipus, Z. (2005). Waveguide miniaturization using uniaxial negative permeability metamaterial, *IEEE Transactions on Antennas and Propagation*, 53(1), 110-119.

Ibraheem, I. A.; & Koch, M. (2007). Coplanar waveguide metamaterials: The role of bandwidth modifying slots, *Applied Physics Letters*, 91(11), 113517-3.

Ibraheem, I. A.; Schoebel, J. & Koch, M. (2008). Group delay characteristics in coplanar waveguide left-handed media, *Journal of Applied Physics*, 103(2), 024903-7.

Iyer, A.; & Eleftheriades, G. (2002). Negative refractive index metamaterials supporting 2-D waves, *IEEE MTT-S International Microwave Symposium Digest*, 2, pp. 1067-1070.

Lagarkov, A. & Kisel, V. (2001). Electrodynamic properties of simple bodies made of materials with negative permeability and negative permittivity. *Doklady Physics*, 46(3), 163-165.

Leonhardt, U. (2006). Optical Conformal Mapping, *Science*, 312(5781), 1777-1780.

Marques, R.; Medina, F. & Rafii-El-Idrissi, R. (2002). Role of bianisotropy in negative permeability and left-handed metamaterials, *Physical Review B*, 65(14), 144440.

Marques, R.; Martin, F. & Sorolla, M. (2008). *Metamaterials with Negative Parameters: Theory, Design, and Microwave Applications: Theory, Design and Microwave Applications*, John Wiley & Sons.

Martin, F.; Falcone, F.; Bonache, J.; Marques, R. & Sorolla, M. (2003a). Miniaturized coplanar waveguide stop band filters based on multiple tuned split ring resonators, *IEEE Microwave and Wireless Components Letters*, 13(12), 511-513.

Martin, F.; Bonache, J.; Falcone, F.; Sorolla, M. & Marques, R. (2003b). Split ring resonator-based left-handed coplanar waveguide, *Applied Physics Letters*, 83(22), 4652-4654.

Oliner, A. A. (2002). A periodic-structure negative-refractive-index medium without resonant elements, *IEEE AP-S/URSI Int. Symp. Dig.*, San Antonio, TX, 41-44.

Pacheco, J.; Grzegorczyk, T. M.; Wu, B.; Zhang, Y. & Kong, J. A. (2002). Power Propagation in Homogeneous Isotropic Frequency-Dispersive Left-Handed Media. *Physical Review Letters*, 89(25), 257401.

Pendry, J. B. (2000). Negative refraction makes a perfect lens, *Physical Review Letters*, 85(18), 3966–3969.

Pendry, J. B.; Holden, A. J.; Stewart, W. J. & Youngs, I. (1996). Extremely low frequency plasmons in metallic mesostructures, *Physical Review Letters*, 76(25), 4773-4776.

Pendry, J. B.; Holden, A. J.; Robbins, D. J. & Stewart, W. J. (1998). Low frequency plasmons in thin-wire structures, *Journal of Physics: Condensed Matter*, 10(22), 4785-4809.

Pendry, J.; Holden, A.; Robbins, D. & Stewart, W. J. (1999). Magnetism from conductors and enhanced nonlinear phenomena, *IEEE Transactions on Microwave Theory and Techniques*, 47(11), 2075–2084.

Pendry, J. B. & Smith, D. R. (2006). The quest for the superlens, *Scientific American*, 295(1), 60-7.

Ramakrishna, S. A.; & Grzegorczyk, T. M. (2008). *Physics and Applications of Negative Refractive Index Materials*, CRC.

Schurig, D.; Mock, J. J.; Justice, B. J.; Cummer, S. A.; Pendry, J. B.; Starr, A. F & Smith, D. R. (2006). Metamaterial Electromagnetic Cloak at Microwave Frequencies. *Science*, 314(5801), 977–980.

Shelby, R. A.; Smith, D. R.; & Schultz, S. (2001). Experimental Verification of a Negative Index of Refraction, *Science*, 292(5514), 77–79.

Simons, R. N. (2001). *Coplanar Waveguide Circuits, Components and Systems*. Wiley-IEEE, New York.

Smith, D. R.; Mock, J. J.; Starr, A. F. & Schurig, D. (2005). Gradient index metamaterials, *Physical Review E*, 71(3), 036609.

Smith, D. R.; Padilla, W. J.; Vier, D. C.; Nemat-Nasser, S. C. & Schultz, S. (2000). Composite Medium with Simultaneously Negative Permeability and Permittivity, *Physical Review Letters*, 84(18), 4184.

Wang, S.; Feresidis, A.; Goussetis, G. & Vardaxoglou, J. C. (2006). High-gain subwavelength resonant cavity antennas based on metamaterial ground planes, *IEE Proceedings-Microwaves, Antennas and Propagation*, 153(1), 1-6.

Wolff, I. (2006). *Coplanar Microwave Integrated Circuits*. John Wiley & Sons.

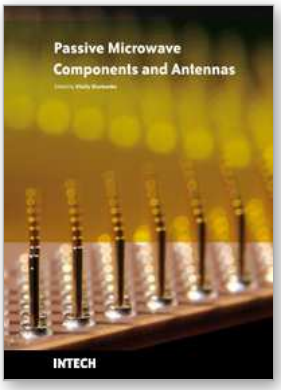

Passive Microwave Components and Antennas

Edited by Vitaliy Zhurbenko

ISBN 978-953-307-083-4
Hard cover, 556 pages
Publisher InTech
Published online 01, April, 2010
Published in print edition April, 2010

Modelling and computations in electromagnetics is a quite fast-growing research area. The recent interest in this field is caused by the increased demand for designing complex microwave components, modeling electromagnetic materials, and rapid increase in computational power for calculation of complex electromagnetic problems. The first part of this book is devoted to the advances in the analysis techniques such as method of moments, finite-difference time- domain method, boundary perturbation theory, Fourier analysis, mode-matching method, and analysis based on circuit theory. These techniques are considered with regard to several challenging technological applications such as those related to electrically large devices, scattering in layered structures, photonic crystals, and artificial materials. The second part of the book deals with waveguides, transmission lines and transitions. This includes microstrip lines (MSL), slot waveguides, substrate integrated waveguides (SIW), vertical transmission lines in multilayer media as well as MSL to SIW and MSL to slot line transitions.

InTech Europe
University Campus STeP Ri
Slavka Krautzeka 83/A
51000 Rijeka, Croatia
Phone: +385 (51) 770 447
Fax: +385 (51) 686 166
www.intechopen.com

InTech China
Unit 405, Office Block, Hotel Equatorial Shanghai
No.65, Yan An Road (West), Shanghai, 200040, China
中国上海市延安西路65号上海国际贵都大饭店办公楼405单元
Phone: +86-21-62489820
Fax: +86-21-62489821